Interaction Mechanism of a Novel Polymer Electrolyte Composed of Poly(acrylonitrile), Lithium Triflate, and Mineral Clay

HSIEN-WEI CHEN, FENG-CHIH CHANG

Institute of Applied Chemistry, National Chiao-Tung University, Hsin-Chu 30043, Taiwan

Received 19 April 2001; revised 8 June 2001; accepted 19 July 2001

ABSTRACT: The addition of optimum cetyl pyridium chloride (CPC)–modified montmorillonite (CM) increases the ionic conductivity of poly(acrylonitrile)-based electrolytes by roughly two orders of magnitude. Specific interactions between the silicate layer, the nitrile group, and the lithium cation were investigated by FTIR, solid-state NMR, dielectric analyzer, and alternating current impedance. IR and NMR spectra confirm that the negative charges in the silicate layers alter the ionic charge environment of the PAN-based electrolyte composites, which have the same function as the polar group in PAN. The optimum CM content to achieve the maximum ionic conductivity is 6 phr. However, untreated montmorillonite leads to insignificant polymer intercalation, the negative charges in the silicate layers fail to appreciably disturb the attractive force of the lithium salt, and the resulting conductivity improvement is also less than that of the CM additives. © 2001 John Wiley & Sons, Inc. J Polym Sci Part B: Polym Phys 39: 2407–2419, 2001

Keywords: polymeric electrolytes; ionic conductivity; clay; PAN

INTRODUCTION

During the past decade, lithium salt–based electrolytes have been the focus of numerous fundamental and application-oriented studies.[1–8] Most Li^+-based polymeric electrolytes have one drawback, that of low ionic conductivity at ambient temperature. One approach to produce electrolytes that possess high conductivity and maintain sufficient performance is to prepare a polymer electrolyte nanocomposite. Because of their small particle size and intercalation property, forming an intercalating polymer in layered inorganic hosts is the most promising method. Numerous studies[9–21] have reported that the high surface area additives, such as ceramic powder and mineral clays, retard the crystallinity of the polymer matrix. Furthermore, given the high amorphous area, the polymer chains are more flexible in the system. Vaia et al.[19] reported that the intercalated clay layers enhance the ionic conductivity of polymeric electrolytes.[18–21] However, this mechanism of enhancement is not clearly understood.

In this work, via solid-state NMR, Fourier transform infrared (FTIR) spectroscopy, dielectric analyzer (DEA), and alternating current (ac) impedance, the complicated interaction between poly(acrylonitrile) (PAN), clay, and lithium triflate salt ($LiCF_3SO_3$) is clarified as an ionic interaction within the solid state. In addition, an increase in ionic conductivity that was observed within the composite system is discussed regarding the formation of contact-ion pairs and higher ionic aggregates. As well, via IR spectra of CN^- and CF_3^- vibrations, the cause of conductivity

Correspondence to: F.-C. Chang (E-mail: changfc@cc.nctu.edu.tw)

Journal of Polymer Science: Part B: Polymer Physics, Vol. 39, 2407–2419 (2001)

variation will be investigated. These vibrations are employed to interpret the formation of the PAN–$LiCF_3SO_3$ complex and ionic aggregates. The purpose of this work is to emphasize the extraordinary effect produced when clay is added to the PAN/Li^+/clay blend system.

EXPERIMENTAL

Materials

Sample Preparation

The poly(acrylonitrile) (PAN) with a weight-average molecular weight of 150,000 was purchased from Polyscience Chemicals. The lithium triflate ($LiCF_3SO_3$) (Aldrich Chemicals, Milwaukee, WI) was dried in a vacuum oven at 80 °C for 24 h and then stored in a desiccator prior to use. DMF was refluxed at a suitable temperature under a nitrogen atmosphere prior to use.

The clay, sodium montmorillonite (1 g), and 50 mL distilled water were placed in a 100-mL beaker, and 0.78 g of cetyl pyridium chloride (CPC) was added to the solution (clay/CPC = 1/2). The mixture was stirred vigorously for 8 h and then filtered and washed with deionized water. The modified clay was dried in a vacuum oven at 60 °C for 24 h. The CPC-modified montmorillonite (CM) was highly hydrophobic.

Preparation of Solid Polymer Electrolyte (SPE)

Dissolving desired amounts of PAN, vacuum-dried $LiCF_3SO_3$ salt, and CM in dry DMF formed PAN–$LiCF_3SO_3$/CM nanocomposites of varying compositions. Following continuous stirring for 24 h at 80 °C, these solutions were maintained at 50 °C for an additional 24 h to remove the solvent, and then further dried under vacuum at 80 °C for a subsequent 3 days. To prevent contact with air and moisture, all nanocomposites were stored in a dry box filled with nitrogen.

Methods

X-ray Measurements

Wide-angle diffraction (WAXD) experiments were conducted on a Rigaku X-ray diffractometer (Rigaku, Japan) that employed Cu Kα radiation (18 kW rotating anode, λ = 1.5405 Å), and were performed at 50 kV and 250 mA with a scanning rate of 2°/min.

Transmission Electron Microscopy (TEM)

TEM photomicrographs of prepared nanocomposites were taken on a JEOL-200FX transmission electron microscope (JEOL, Japan) that was operating at 200 kV of accelerated voltage.

FTIR Measurements

The conventional NaCl disk method was employed to measure infrared spectra of composite films. All polymer films were prepared within an N_2 atmosphere. The DMF solution was cast onto a NaCl disk, from which the solvent was removed under vacuum at 70 °C for 48 h. All infrared spectra were obtained in the range of 4000–600 cm^{-1} within a Nicolet AVATRR 320 FTIR spectrometer (Nicolet Instruments, Madison, WI) with a 1 cm^{-1} resolution.

NMR Characterizations

High-resolution solid-state ^7Li NMR spectra were recorded on a Bruker DSX-400 spectrometer (Bruker Instruments, Billerica, MA) at a resonance frequency of 155.5 MHz. The ^7Li magic angle spinning (MAS) spectra were measured with 3-μs 90° pulse angle, 2-s pulse delay time, 2048 scans, and spinning speed 3 kHz. All NMR spectra were recorded at 300 K with proton decoupling and MAS of 10 kHz.

Dielectric Constant Analyses

A TA Instruments DEA 2970 (TA Instruments, New Castle, DE) at 100 Hz was employed to measure the dielectric constant of the composite at varying temperatures (50 to 150 °C). The specimen thickness varied from 0.25 to 0.3 mm.

Conductivity Measurements

Alternating current ionic conductivities were measured on an AUTOLAB designed by Eco Chemie within the frequency range from 10 MHz to 10 Hz. The composite film was sandwiched between stainless steel blocking electrodes (1 cm diameter). The specimen thickness varied from 0.8 to 1.2 mm, and the impedance response was recorded between 30 and 120 °C.

RESULTS AND DISCUSSION

Dispersion of Clay in the PAN Matrix

The X-ray diffraction patterns for the dried clay (MMT) and the CPC-modified montmorillonite

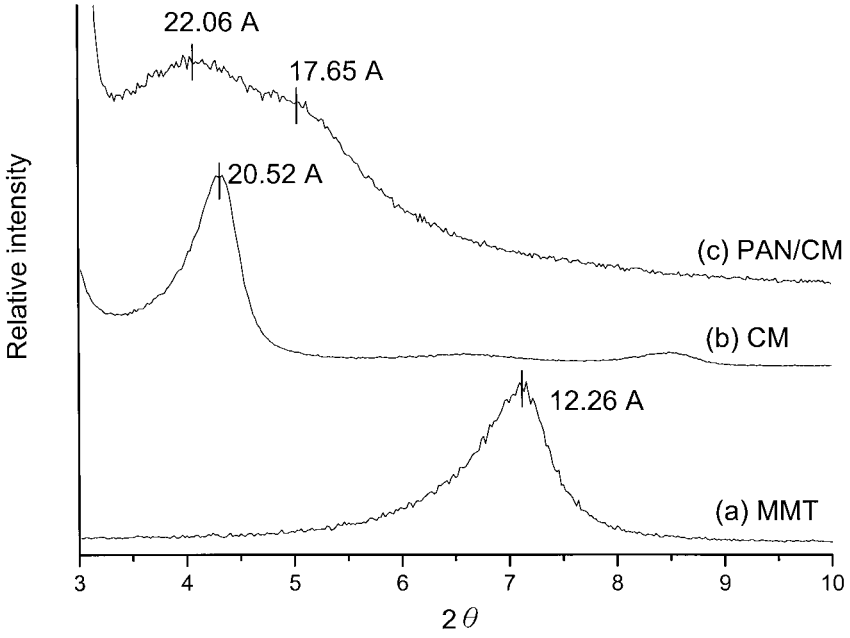

Figure 1. WAXD patterns of (a) MMT, (b) CM, and (c) polymer nanocomposite with 8 phr CM.

(CM) are presented in Figure 1(a) and (b). Upon intercalation, the basal spacing expanded from 12.3 to 20.5 Å, indicating the incorporation of large surfactant molecules, as displayed in **Scheme 1**. Figure 1(c) presents the X-ray pattern of PAN with 8 phr CM nanocomposite with a broad diffraction peak. The large broadening peak with a higher interlayer spacing (22.06–17.56 Å) indicates that intercalation of the polymer chains further expends the interlayer spacing within the galleries.

Scheme 1 shows that the hydrated cations are exchanged with bulky alkylammonium molecules to form larger interlayer spacing. The modified clay (CM) is organophilic with a lower surface energy, which is more compatible with organic polymers. The polymer chains intercalate within the galleries as a result of the negative surface charge, and the cationic head group of the alkylammonium molecule preferentially resides on the layer surface.

Scheme 1 does not depict the construction of the incorporated surfactant molecules within the silicate layers. The molecular length of CPC, calculated by constructing the completely structure space filling (CPK) model, is 22.945 Å. When the sum of the calculated molecular length and a silicate layer with the observed basal spacing are compared, it is anticipated that the CPC is oriented diagonally within the silicate layers of MMT (**Scheme 2**). The angle of CPC slant to the MMT layer α is calculated based on the following equation:

$$\sin \alpha = (d - 10)/L, \quad \alpha = 15.721°$$

where L is the molecular length of the CPC and d is the basal spacing.

TEM was employed to further characterize nanocomposite morphologies. Figure 2 illustrates TEM images of PAN/CM nanocomposites with CM contents of 8 and 14 phr. Examination of these TEM photomicrographs reveals stacked silicate layers. At a higher filler content (14 phr CM), well-exfoliated and better-dispersed nanosized sheets are observed. These ordered aggregates are separated randomly (50–1500 Å) and delaminated layers are separated by approximately 20–25 Å. Furthermore, a certain fraction of the CM layers is embedded in the polymer matrix, to form a completely exfoliated arrangement.

Infrared Spectra

Because the nitrile group is a strong electron donor, within the PAN-based polymer electrolyte, the Li^+ ion tends to complex with the nitrogen atom of the nitrile group (CN^-). Infrared is a powerful tool to monitor ionic association. Accord-

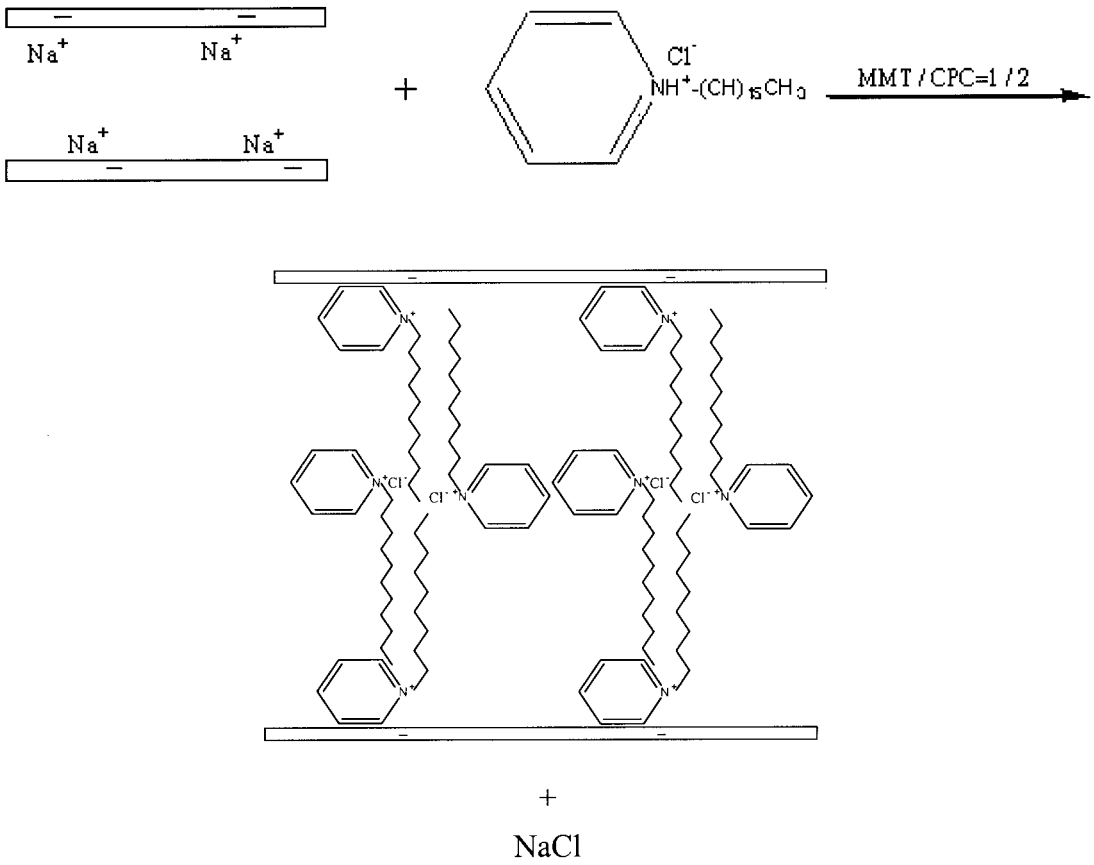

Scheme 1. Proposed model of the intercalation of CPC surfactant into smectite MMT galleries.

ing to previous publications,[21–26] the peak at 2243 cm^{-1} in Figure 3 represents the free C≡N group of PAN. When the lithium triflate was added, a small peak corresponding to the interaction between the lithium cation and the C≡N group appears at 2269 cm^{-1}. When the CM content in $(PAN)_8LiCF_3SO_3$/CM system is varied, the shoulder at 2269 cm^{-1} does not shift, although the relative band intensity increases with increasing CM content. This observation indicates that the presence of the CM enhances the interaction of the PAN polar group with the lithium cation.

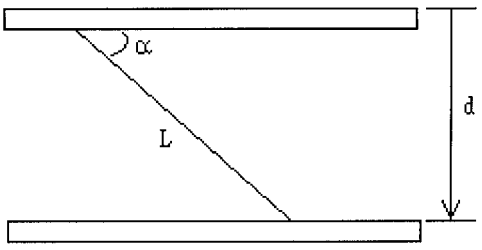

Scheme 2. Mode of CPC molecule between layers of montmorillonite.

The $\delta_s(CF_3)$ internal mode of the $CF_3SO_3^-$ anion displays an identical trend. This internal mode is particularly sensitive to the local anionic environment.[22,27–29] The corresponding band, which originated from the triflate ion $\delta_s(CF_3)$ mode, reflects the dissolution of the triflate ionic species in the PAN. The corresponding intensity of the $\delta_s(CF_3)$ mode provides quantitative information regarding various anionic species distribution. Many studies[28,30,31] have attributed the components at about 752, about 758, and 763 cm^{-1} from other polymer–lithium triflate systems to free anions, ion pairs, and $Li_2CF_3SO_3^+$ triple ions, respectively. Figure 4 presents IR spectra of the $\delta_s(CF_3)$ mode as a function of CM concentration for the $(PAN)_8LiCF_3SO_3$/CM system, in which a large absorption band at about 770 cm^{-1} and a broad component at about 766 cm^{-1} appear. With an increase in CM concentration, these $\delta_s(CF_3)$ bands do not show any evidence of dissociation of these species into spectroscopically free anions. The chief band at about 770 cm^{-1} displayed in Figure 4(a) is attributed to the $CF_3SO_3^-$ anion

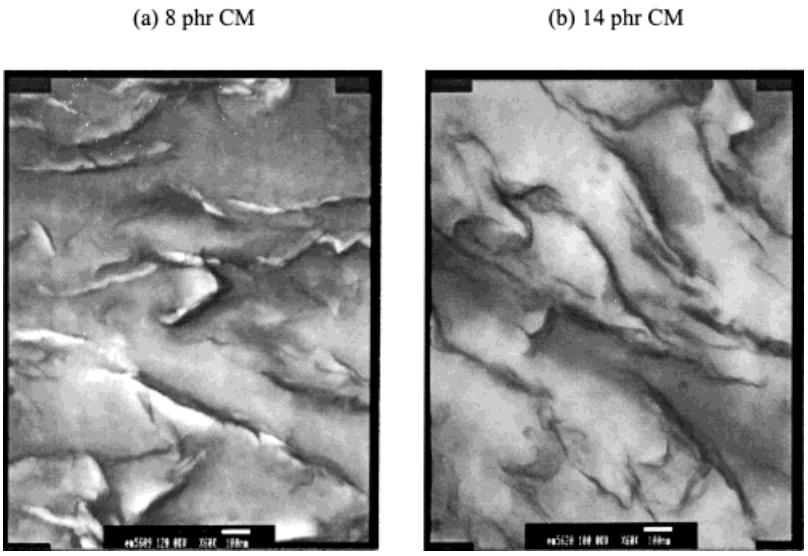

Figure 2. TEM micrograph (×60K) of PAN filled with various CM concentrations (1 mm = 600 nm): (a) 8 phr, (b) 14 phr.

interacting extensively with lithium cations, an indication of larger ionic aggregations. The relative broad and minor component at 766 cm^{-1} comes from the ion-pair species. An increase in CM concentration, as presented in Figure 4, increases the 766 cm^{-1} ion-pair band at the expense of the larger ionic aggregate component at 770 cm^{-1}. These IR trends of the $\delta_s(CF_3)$ mode confirm that the CM facilitates CN group interaction with the lithium ion and causes reduction of the attractive force between cationic and anionic ions of $LiCF_3SO_3$.

Figures 3 and 4 depict the dramatic changes of IR spectra, which confirm that the addition of CM significantly influences the entire cationic charge environment. The negative charge in the silicate

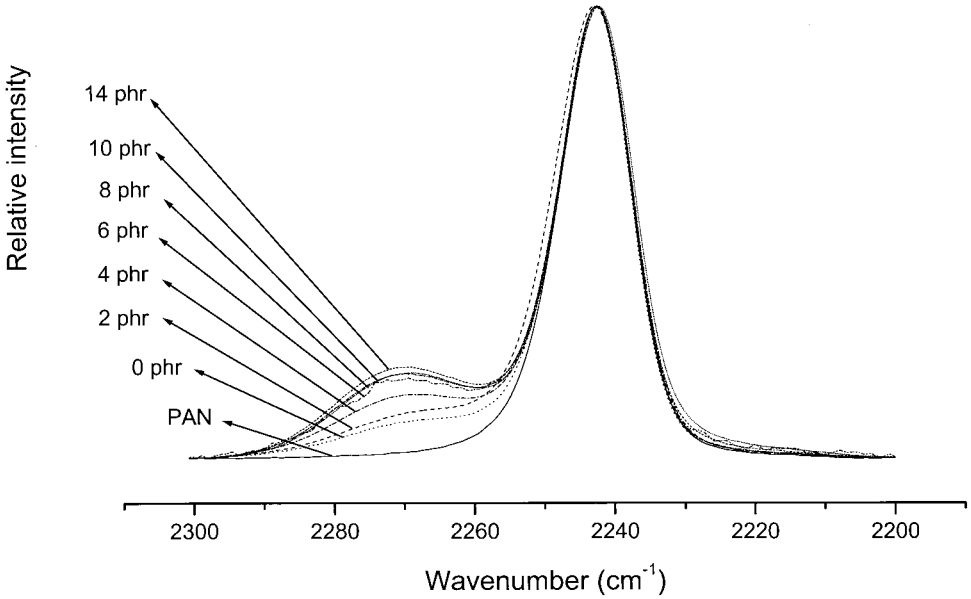

Figure 3. Infrared spectra of the symmetric nitrile-stretching mode (C≡N group) of PAN-based nanocomposite and $LiCF_3SO_3$ composite electrolytes. [PAN]/[$LiCF_3SO_3$] equivalent ratio = 8, containing various CM contents.

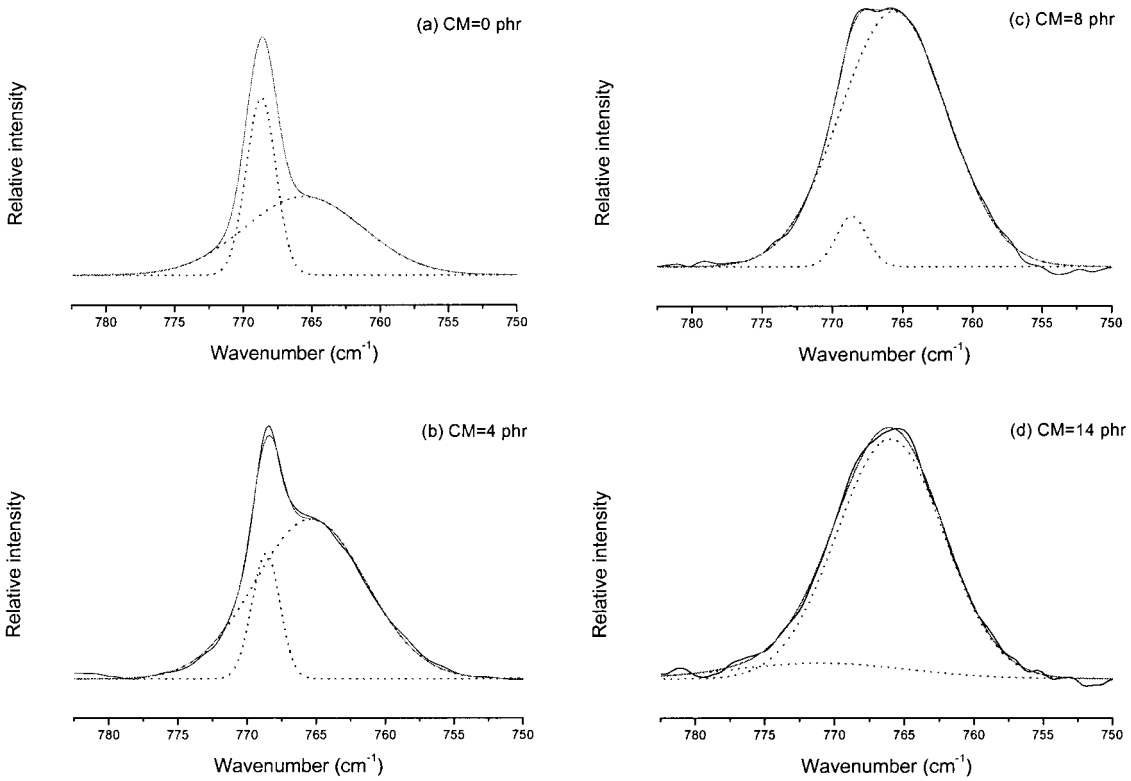

Figure 4. Infrared spectra of $\delta_s(CF_3)$ internal modes of PAN-based composite electrolytes. [PAN]/[$LiCF_3SO_3$] equivalent ratio = 8, containing various CM contents: (a) 0 phr, (b) 4 phr, (c) 8 phr, (d) 14 phr.

surface layers interacts with the lithium cation and plays the same role as that of the polar group in PAN. Based on this knowledge regarding the $(PAN)_8LiCF_3SO_3$/CM composite microstructure, the total structural geometry of this PAN-based polymer electrolyte is depicted in **Scheme 3**. The surface energy of the modified organophilic clays (CM) is lower relative to that of the untreated clay and becomes more compatible with organic polymers. Therefore, polymer chains can intercalate more easily within the clay galleries. The incorporation mechanisms of polymer chains are presented in **Scheme 3(a)** and **(b)**. **Scheme 3(c)** depicts the polymer electrolyte nanocomposite, in which the lithium triflate diffuses into the PAN/CM composite. **Scheme 3(c)** also illustrates the lithium cation interaction with polar groups of the PAN, the silicate layers, and anionic ions. When **Scheme 3(c)** and the experimental findings from the IR spectra are compared, the negative charges in the silicate layers are expected to reduce the attractive force of the $Li^+ \cdots CF_3SO_3^-$. By weakening the attractive force within the lithium salt, these CN polar groups are able to interact more easily with lithium cations, as confirmed by previous IR spectra (Fig. 3).

It is concluded that the charged environment of the $(PAN)_8LiCF_3SO_3$/CM composite has changed as a result of acid–base interactions that involved the CN polar group, filler base, and alkali metal cations. The clay filler alters the fraction of the available CN sites, which in turn changed the formation of varying ionic types (free ions, ion-pairs, or ionic aggregates).

In Figure 5, the adsorption band of PAN at about 1662 cm^{-1} can be attributed to the free C═O of the residual solvent DMF. For the $(PAN)_8LiCF_3SO_3$ membrane, the appearance of other adsorption band at the lower frequency of about 1633 cm^{-1} is at the expense of the free C═O group ($\sim$ 1662 cm^{-1}). The interaction between lithium cations and C═O reduces the free C═O adsorption band ($\sim$ 1662 cm^{-1}). However, the intensity of the interaction band ($\sim$ 1633 cm^{-1}) decreases gradually with increasing CM content. This decreased intensity at about 1633 cm^{-1} confirms that the silicate layers interact with the lithium cation and thus reduce the ex-

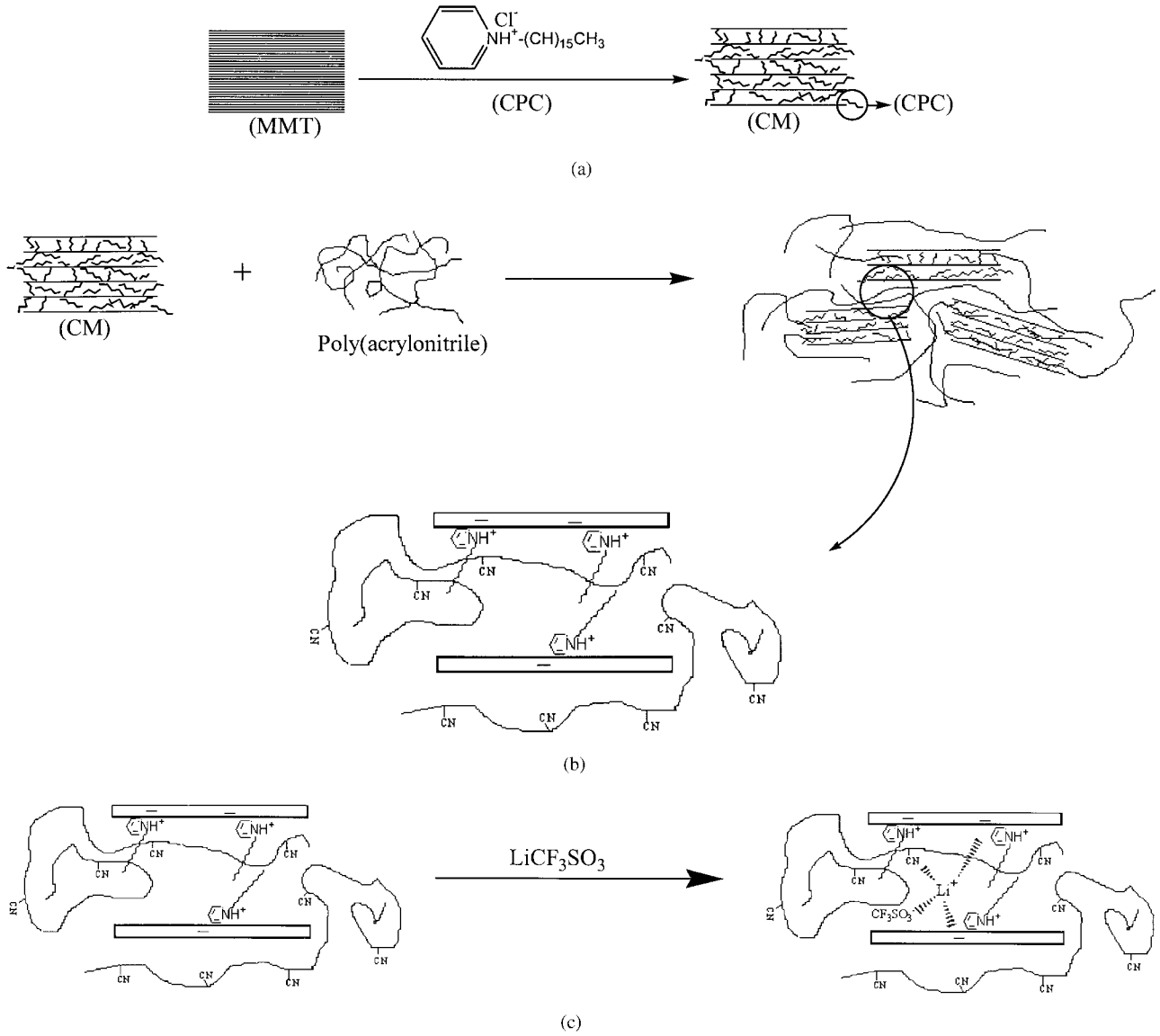

Scheme 3. Schematic representations of (a) CM modification with CPC; (b) incorporation of PAN into CM layers, producing PAN-based nanocomposite; and (c) incorporation of the PAN-based nanocomposite with lithium triflate ($LiCF_3O_3$) to form polymer electrolyte.

tent of C═O group interacting with the lithium cation.

NMR Experiments

The ^{7}Li solid-state NMR spectrum was employed to characterize the interaction behavior in $(PAN)_8LiCF_3SO_3$/CM electrolyte nanocomposites. Figure 6 presents the scale-expanded ^{7}Li magic angle spinning (MAS) NMR spectra with high-power proton decoupling and the corresponding peak assignments of various CM concentrations in the $(PAN)_8LiCF_3SO_3$/CM system. With the addition of CM, the lithium cation peak of the lithium triflate shifts dramatically downfield, thus reflecting the complex interaction strength. This observed chemical shift increases with an increase in CM concentration, implying that CM is a strong electron donor that interacts with lithium cations and thus decreases nucleus shielding.

Dielectric Property

As is well known, adding a plasticizer with a higher dielectric constant than that of the poly-

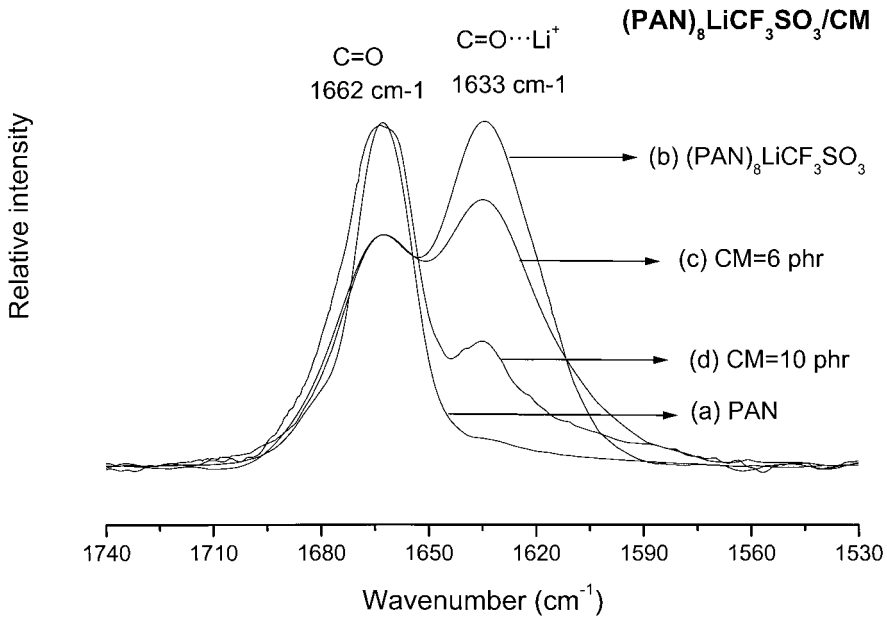

Figure 5. Infrared spectra of C═O groups in PAN-based composite electrolytes. [PAN]/[$LiCF_3SO_3$] equivalent ratio = 8, containing various CM contents: (a) PAN; (b) $(PAN)_8LiCF_3SO_3$; (c) CM = 6 phr; (d) CM = 10 phr.

mer host facilitates ion dissociation and increases the number of available charge carriers. Thus, the dielectric constant is of particular significance to ionic conducting polymers. Clay is a natural mineral with high dielectric constant. Therefore, if the plasticizer is replaced with clay, polar groups

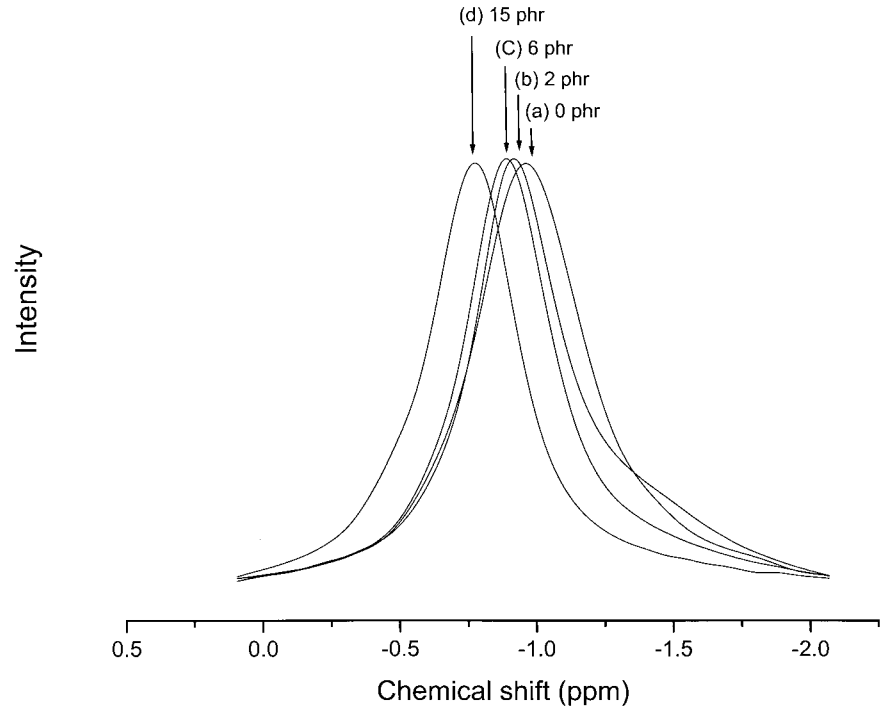

Figure 6. Scaled ^7Li CP/MAS NMR spectra region of PAN-based composite electrolytes. [PAN]/[$LiCF_3SO_3$] equivalent ratio = 8, containing various CM contents: (a) 0 phr, (b) 2 phr, (c) 6 phr, (d) 15 phr.

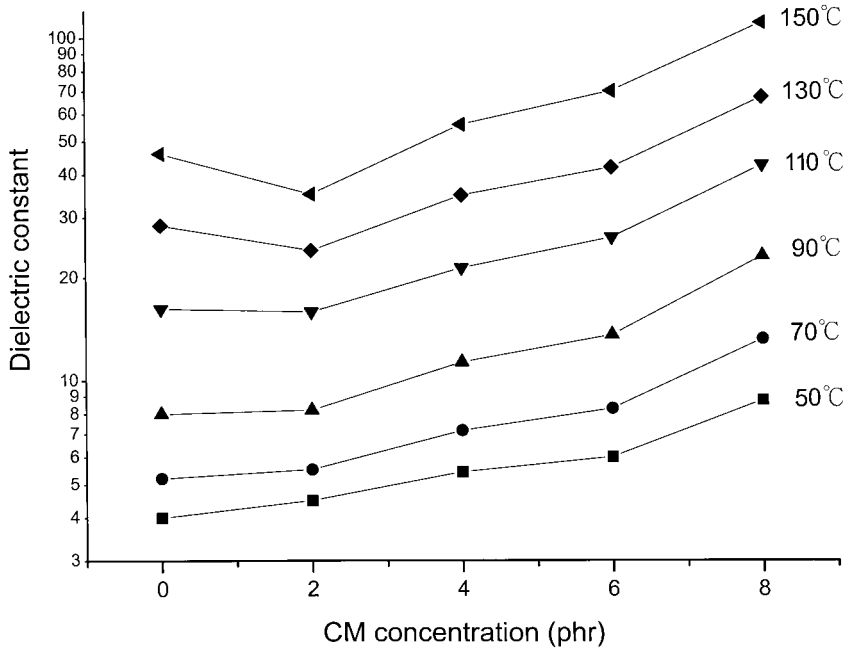

Figure 7. Dependency of dielectric constant of PAN/CM nanocomposites with various levels of CM on temperature: (■) 50 °C; (●) 70 °C; (▲) 90 °C; (▼) 110 °C; (◆) 130 °C; (◀) 150 °C.

in the polymer can be enhanced to facilitate lithium salt ion dissociation. To confirm this assumption, the dielectric behavior of the PAN/CM blends without the lithium salt must be obtained. Figure 7 presents the effect of CM concentration on the PAN dielectric constant when temperatures are varied from 50 to 150 °C at a constant 100 Hz. These curves indicate that, at all temperatures investigated, the dielectric constant increases as the CM concentration is increased. Table I presents values of the dielectric constant with varying CM contents and temperatures. For example, the dielectric constant of the blank PAN at 50 °C is 4, which increases to 8.77 with 8 phr CM. The change in dielectric constant can be attributed to the dipole within the silicate layers. The composite containing a lower CM content contains smaller dipoles, which orient in the direction of the applied field. Alternately, the composite with high CM and a greater fraction of silicate layers contains more negative charges (dipoles), which orient in the direction of the applied field, resulting in a higher dielectric constant. Given the higher mobility of the polymer matrix, higher temperatures also result in higher dielectric constant of the composite, as would be expected.

Conductivity

Figure 8 presents Arrhenius plots of the temperature dependency of the ionic conductivity for the

Table I. Dielectric Constant for PAN/CM Hybrid as a Function of CM Additive

Composition (CM, phr)	Dielectric Constant					
	50 °C	70 °C	90 °C	110 °C	130 °C	150 °C
0	4.00	5.20	8.00	16.2	28.40	46.00
2	4.49	5.52	8.21	15.89	24.03	35.09
4	5.43	7.16	11.31	21.33	34.78	55.82
6	6.00	8.29	13.59	26.17	41.90	69.90
8	8.77	13.22	23.11	42.60	67.10	110.60

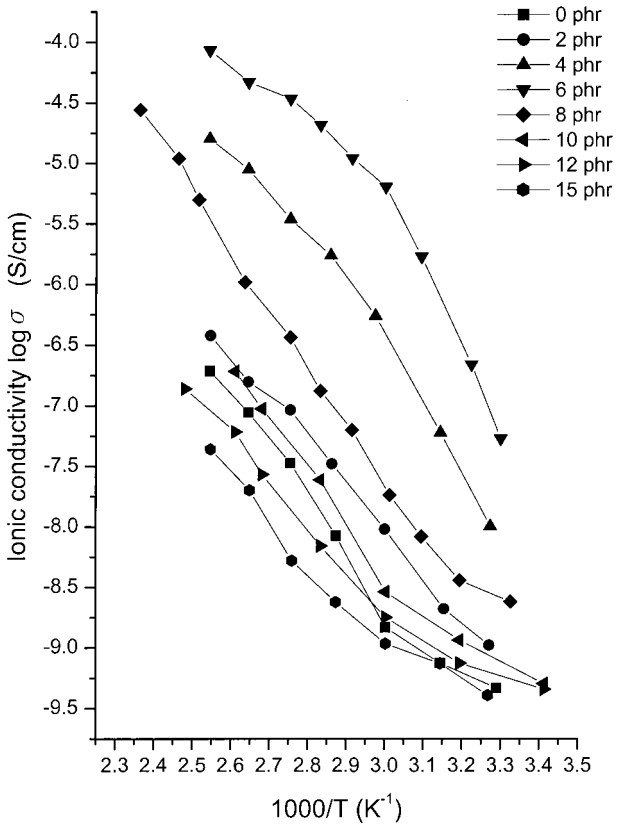

Figure 8. Arrhenius conductivity plots of PAN-based composite electrolyte containing various contents of CM: (■) 0 phr; (●) 2 phr; (▲) 4 phr; (▼) 6 phr; (◆) 8 phr; (◀) 10 phr; (▶) 12 phr; (●) 15 phr (where [PAN]/[$LiCF_3SO_3$] equivalent ratio = 8).

$(PAN)_8LiCF_3SO_3$/CM electrolyte nanocomposites containing various CM concentrations. Conductivity varies with the CM content by several orders of magnitude. Also, conductivity increases with an increase in CM content and attains a maximum value when the CM concentration is 6 phr. Subsequently, the conductivity decreases gradually with further increase in CM content.

Figure 9 presents the conductivity versus CM content for the $(PAN)_8LiC_3SO_3$/CM electrolyte nanocomposites at various temperatures. A considerable increase in conductivity is observed when the CM additives are added and the maximum ionic conductivity is achieved at the CM concentration of 6 phr. When the CM is increased to 8 phr, the conductivity drastically decreases to its original value. With a further increase in CM content, the conductivity decreases even below the original value. Figure 10 presents the conductivity versus untreated clay (clay untreated by CPC). These results show a trend similar to trends depicted in Figure 9. However, the extent of ionic conductivity increase is substantially less, compared to that of the CM system, whereas the maximum conductivity is at 10 phr of the untreated clay. That means the critical clay content of the untreated clay is at 10 phr, which is higher than that of the CM system at 6 phr.

Table II summaries all data on ionic conductivity. At 40 °C and 6 phr CM, the conductivity is approximately 80-fold higher than that of the plain $(PAN)_8LiCF_3SO_3$ system. However, in the untreated clay additives system at 40 °C, the maximum conductivity occurs at 10 phr, only twofold that of the plain system. The negative charges in the silicate layers interact with lithium cations and disturb the attractive force between the cationic and anionic ions of the lithium salt. Nevertheless, an excess of CM (excess 6 phr CM) may tightly bind lithium cations, thus restricting cationic mobility and decreasing its ionic conductivity. The conductivity data imply that the addition of an optimized CM content (6 phr) is able to drastically enhance the ionic conductivity and to form the equilibrium attractive force in the system, resulting in the highest cationic mobility. In the system with untreated clay additives with significantly low polymer intercalation, the negative charges in the silicate layers have limited ability to disturb the attractive force of the lithium salt. Thus, to achieve maximum ionic conductivity, a greater quantity of the untreated clay (10 phr) is required and the resulting conductivity improvement of the untreated clay is also substantially less. To further clarify the effect from the silicate layers, it is necessary to compare the conductivity with different CPC concentrations. Figure 11 presents the conductivity versus concentration of CPC in CM, from which it is clear that the conductivity is independent of the CPC concentration. This result indirectly verifies the specific interaction between montmorillonite and the lithium cation.

CONCLUSIONS

This study demonstrated that the addition of an optimum content of CPC-modified montmorillonite increases ionic conductivity of the poly(acrylonitrile)-based electrolytes by nearly two orders of magnitude over that of the plain $(PAN)_8LiCF_3SO_3$ system. FTIR, solid-state NMR, and DEA studies indicated that strong interactions occur between

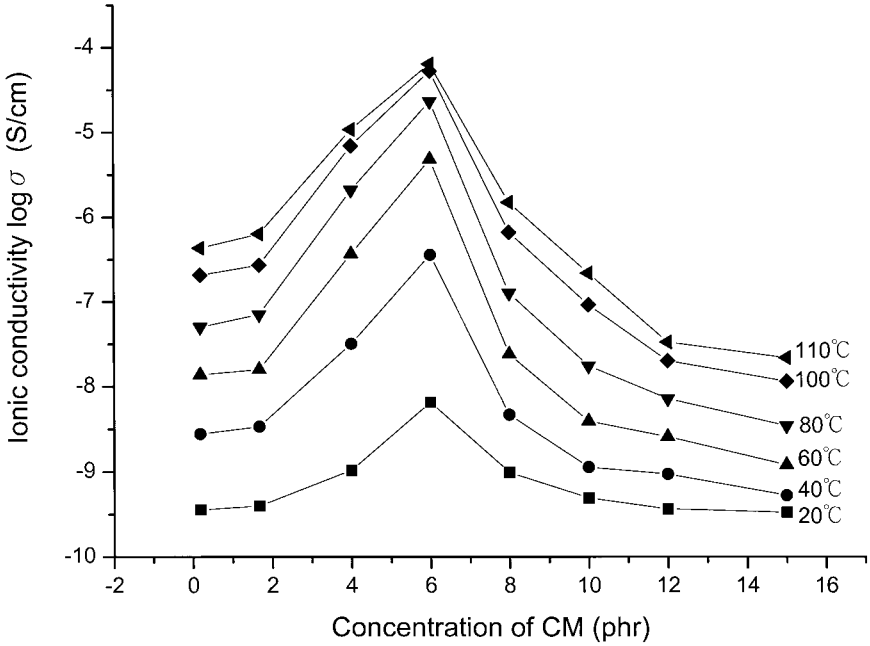

Figure 9. Dependency of ionic conductivity of PAN-based composite electrolyte containing various CM contents at the same temperature: (■) 20 °C; (●) 40 °C; (▲) 60 °C; (▼) 80 °C; (◆) 100 °C; (◀) 110 °C (where [PAN]/[LiCF$_3$SO$_3$] equivalent ratio = 8).

the silicate layer and the dopant salt LiCF$_3$SO$_3$ within the (PAN)$_8$LiCF$_3$SO$_3$/CM system. The negative charges in the silicate surface layers interact with lithium cation to form various complexes and play the same role as does the polar group in PAN. The presence of these complexes tends to

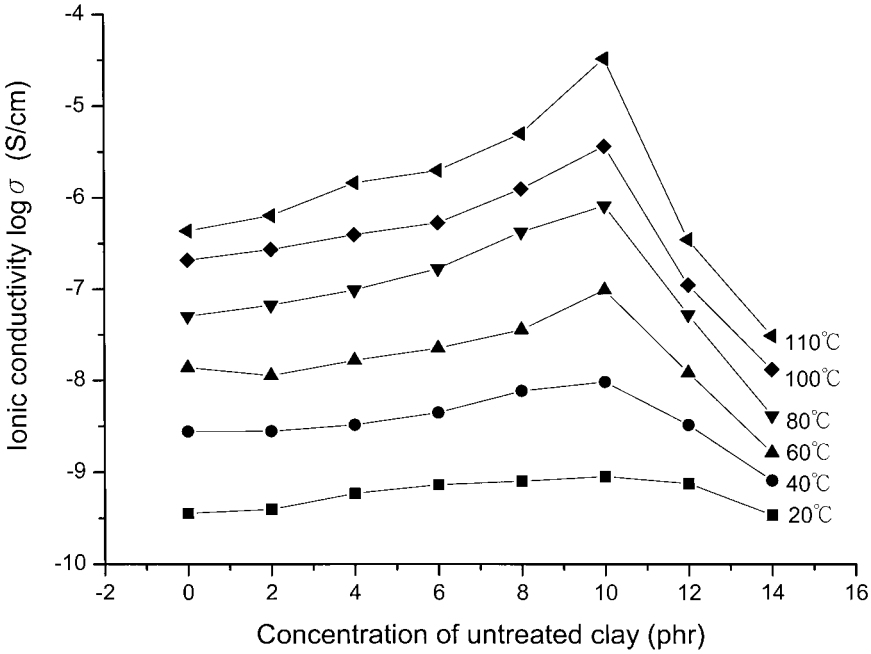

Figure 10. Dependency of ionic conductivity of PAN-based composite electrolyte containing various untreated clay contents at the same temperature: (■) 20 °C; (●) 40 °C; (▲) 60 °C; (▼) 80 °C; (◆) 100 °C; (◀) 110 °C (where [PAN]/[LiCF$_3$SO$_3$] equivalent ratio = 8).

Table II. Compare of the Ionic Conductivity for PAN-Based Nanocomposites Electrolyte as a Function of CM Additives and Untreated Clay Additives[a]

Additives Concentration (phr)	Conductivity of CM Added System (S/cm × 10^7)					Conductivity of Untreated Clay Added System (S/cm × 10^7)				
	40 °C	60 °C	80 °C	100 °C	110 °C	40 °C	60 °C	80 °C	100 °C	110 °C
0	0.047	0.138	0.502	2.068	4.313					
2	0.052	0.097	0.404	1.364	2.351	0.028	0.113	0.663	2.713	6.343
4	0.318	3.694	20.927	69.467	108.104	0.033	0.165	0.974	3.919	14.508
6	3.597	48.174	231.377	525.352	637.470	0.044	0.225	1.676	5.324	19.796
8	0.047	0.240	1.266	6.614	14.947	0.077	0.357	4.222	12.447	49.856
10	0.011	0.039	0.175	0.918	2.180	0.096	0.974	8.140	36.378	326.069
12	0.026	0.026	0.072	0.201	0.334	0.033	0.121	0.525	1.106	3.482
15	0.005	0.012	0.035	0.115	0.218	0.008	0.016	0.041	0.131	0.307

[a] [PAN]/[$LiCF_3SO_3$] equivalent ratio = 8.

reduce the attractive force between the lithium cation and anion, producing a highly conductive phase and higher system conductivity. The optimum CM content to achieve maximum ionic conductivity is 6 phr. For the untreated clay system with significantly lower polymer intercalation and lower negative charges in the silicate layers, it is unable to disturb appreciably the attractive force of the lithium salt, and the subsequent conductivity improvement is also substantially less than that of the CM additives. The balanced attractive forces among silicate layers, nitrile groups, and lithium cation produce an optimum ionic conductivity.

The authors thank the Chinese Petroleum Corp. of the Republic of China for financially supporting this research under Contract No. NSC 89-CPC-7-009-007.

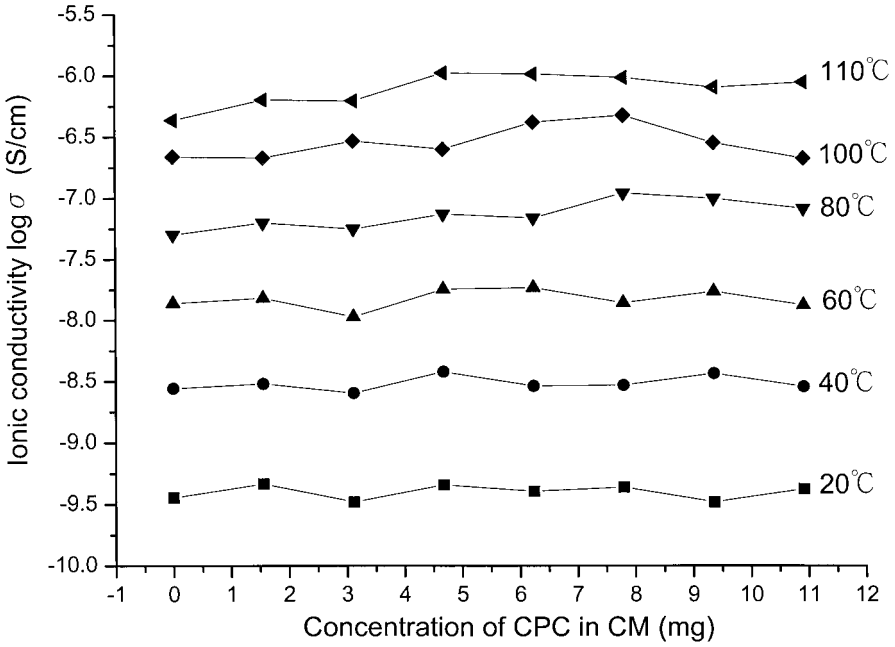

Figure 11. Dependency of ionic conductivity of PAN-based composite electrolyte containing various CM contents at the same temperature: (■) 20 °C; (●) 40 °C; (▲) 60 °C; (▼) 80 °C; (◆) 100 °C; (◀) 110 °C (where [PAN]/[$LiCF_3SO_3$] equivalent ratio = 8).

REFERENCES AND NOTES

1. Scrosati, B. In Polymer Electrolyte Reviews; MacCallum, J. R.; Vincent, C. A., Eds.; Elsevier Applied Science: New York, 1989; p 315.
2. Scrosati, B. In Applications of Electroactive Polymers; Scrosati, B., Ed.; Chapman & Hall: New York, 1993; p 251.
3. Armand, M. B. Solid State Ionics 1983, 9/10, 745.
4. Chao, S.; Wrighton, M. S. J Am Chem Soc 1987, 109, 2197.
5. Fenton, D. E.; Parker, J. M.; Wright, P. V. Polymer 1973, 7, 319.
6. Ratner, M. A.; Shriver, D. F. Chem Rev 1988, 88, 109.
7. Wang, L.; Yang, B.; Wang, X. L.; Tang, X. Z. J Appl Polym Sci 1999, 71, 1711.
8. Wang, X. L.; Li, H.; Tang, X. Z.; Chang, F. C. J Appl Polym Sci Part B: Polym Phys 1999, 37, 837.
9. Croce, F.; Curini, R.; Martinelli, A.; Persi, L.; Ronci, F.; Scrosati, B.; Caminiti, R. J Phys Chem B 1999, 103, 10632.
10. Kumar, B.; Scanlon, L. G. Solid State Ionics 1999, 124, 239.
11. Ponomareva, V. G.; Lavrova, G. V.; Simonova, L. G. Solid State Ionics 1999, 119, 295.
12. Best, A. S.; Ferry, A.; MacFarlane, D. R.; Forsyth, M. Solid State Ionics 1999, 126, 269.
13. Croce, F.; Appetecchi, G. B.; Persi, L.; Scrosati, B. Nature 1998, 394, 456.
14. Wieczorek, W.; Raducha, D.; Zalewska, A.; Stevens, J. R. J Phys Chem B 1998, 102, 8725.
15. Kloster, G. M.; Thomas, J. A.; Brazis, P. W.; Kannewurf, C. R.; Shriver, D. F. Chem Mater 1996, 8, 2418.
16. Wieczorek, W.; Florjanczyk, Z.; Stevens, J. R. Electrochim Acta 1995, 40, 2251.
17. Wieczorek, W.; Such, K.; Chung, S. H.; Stevens, J. R. J Phys Chem 1994, 98, 9047.
18. Ogata, N.; Kawakage, S.; Ogihara, T. Polymer 1997, 38, 5115.
19. Vaia, R. A.; Vasudevan, S.; Krawiec, W.; Scanlon, L. G.; Giannelis, E. P. Adv Mater 1995, 7, 154.
20. Jeevanandam, P.; Vasudevan, S. Chem Mater 1998, 10, 1276.
21. Wong, S.; Zax, D. B. Electrochim Acta 1997, 42, 3513.
22. Ferry, A.; Edman, L.; Forsyth, M.; MacFarlane, D. R.; Sun, J. Electrochim Acta 2000, 45, 1237.
23. Wang, Z.; Huang, B.; Xue, R.; Huang, X.; Chen, L. Solid State Ionics 1999, 121, 141.
24. Huang, B.; Wang, Z.; Chen, L.; Xue, R.; Wang, F. Solid State Ionics 1996, 91, 279.
25. Wang, Z.; Huang, B.; Huang, H.; Xue, R.; Chen, L.; Wang, F. Spectrochim Acta Part A 1996, 52, 691.
26. Huang, B.; Wang, Z.; Li, G.; Huang, H.; Xue, R.; Chen, L.; Wang, F. Solid State Ionics 1996, 85, 79.
27. Ferry, A.; Edman, L.; Forsyth, M.; MacFarlane, D. R.; Sun, J. J Appl Phys 1999, 86, 2346.
28. Ferry, A. J Phys Chem B 1997, 101, 150.
29. Huang, W.; Frech, R. Polymer 1994, 35, 235.
30. Huang, W.; Frech, R.; Wheeler, R. A. J Phys Chem 1994, 98, 100.
31. Frech, R.; Chintapalli, S.; Bruce, P. G.; Vincent, C. A. Chem Commun 1997, 157.